Optical Trapping and Two-Photon Excitation of Colloidal Quantum Dots using Bowtie Apertures

Russell A. Jensen,[†,§] I-Chun Huang,[‡,§] Ou Chen,[†] Jennifer T. Choy,[¶] Thomas S. Bischof,[†] Marko Lončar,[*,¶] and Moungi G. Bawendi[*,†]

[†]*Department of Chemistry, Massachusetts Institute of Technology, Cambridge, Massachusetts 02139, USA*

[‡]*John A. Paulson School of Engineering and Applied Sciences, Harvard University, Cambridge, Massachusetts 02138, USA*

[¶]*School of Engineering and Applied Science, Harvard University, Cambridge, Massachusetts 02138, USA*

[§]*These authors contributed equally to this work.*

E-mail: loncar@seas.harvard.edu; mgb@mit.edu

S1 Silica Coated Quantum Dot (scQD) Synthesis and Characterization

Core/shell CdSe/CdS colloidal quantum dots (QDs) were synthesized as previously described.[1,2] Silica overcoating was performed by loading 30 mL anhydrous cyclohexane into a 100 mL round bottom flask. Under vigorous stirring, 4.75 mL of Igepal CO-520 was added. After stirring for 10 minutes, 1 mL of QD-cyclohexane solution (3 μM) was injected into the reaction followed by slowly adding 150 μL tetraethyl orthosilicate (TEOS, 99%). After another 10 minutes of stirring, 0.5 mL of ammonium hydroxide solution (28% in water)

was injected dropwise into the solution. The final reaction solution was stirred for 18 hr at room temperature before purifying the scQDs via precipitation using ethanol (∼20 mL) and collecting by centrifugation. The scQDs were washed with ethanol twice more and finally dissolved into 2 mL DI-water before storage at 4°C until use. Normalized absorption and emission spectra are shown in figure S1.

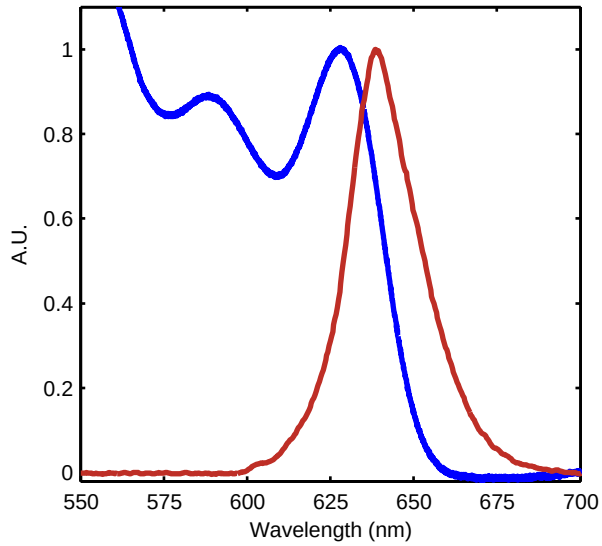

Figure S1: Normalized absorption (blue) and emission (red) spectra for scQDs. Continuous wave 532 nm excitation was used as an excitation source for the emission spectrum.

Prior to some measurements, the scQD solution was passed through a 20 nm pore syringe filter (Whatman) to reduce the mean particle diameter. Dynamic light scattering (DLS) was performed on filtered and unfiltered particles and results calculated by volume are plotted in supplementary figure S2. Mean hydrodynamic diameters are 21.1 nm and 39.2 nm for filtered and unfiltered particles, respectively. It should be noted that because DLS measures the hydrodynamic diameter of particles, these results are likely an overestimation of the actual particle sizes.

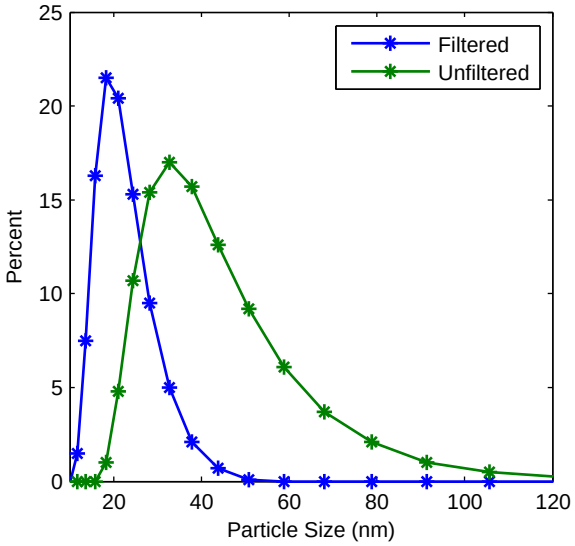

Figure S2: Size distribution of scQDs before (green) and after (blue) filtering measured with DLS. Sizes were calculated by volume.

S2 Aperture Fabrication

Bowtie apertures were fabricated using a lift-off procedure on a 100 nm thick silicon nitride (SiN) membrane with a silicon scaffold from Norcada Inc. The SiN substrate was spin-coated with Hydrogen silsesquioxane (HSQ), a negative tone electron-beam resist (FOX-16, Dow Corning), and bowties were patterned with e-beam lithography (Elionix ELS-F125). The sample was developed in tetramethylammonium hydroxide for 17 seconds, leaving behind 800 nm tall bowtie posts. Electron bean evaporation (Denton) was used to evaporate a 2 nm layer of titanium followed by a 130 nm layer of silver. The sample was briefly scrubbed with a swab prior to performing a 130 second, 5:1 buffered oxide etch. Scrubbing the sample is crucial for high device yield because it breaks posts extending above the silver surface that may have metal particles deposited on the sidewalls. Even though e-beam deposition is directional, a small amount of sidewall deposition is unavoidable and causes incomplete lift-off and poor device fabrication. A schematic of the lift-off procedure is presented in figure S3a.

By this scalable fabrication technique we can realize thousands of devices on a single

chip. For example, the aperture array in figure S3b can be easily fabricated with gaps as small as 8nm in 90nm thick silver layer. This is very challenging to accomplish using focused ion beam milling. Also, a 3D sketch of our device is illustrated in figure S4.

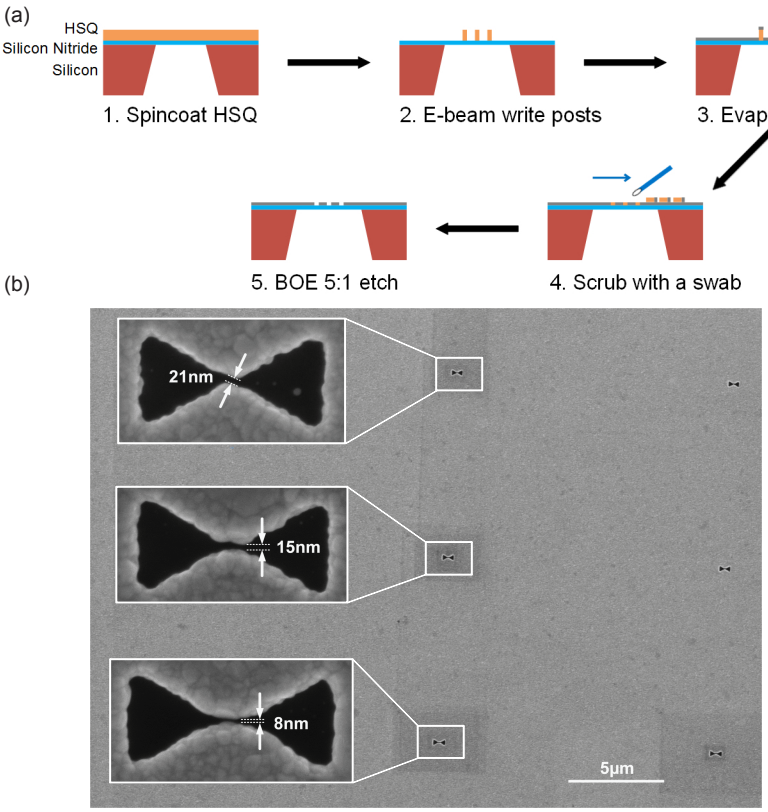

Figure S3: (a) Lift-off procedure schematic. (b) The bowtie aperture array showing the capability of this fabrication method: implement large amount of small-gap apertures by e-beam lithography and lift-off.

S3 56 nm Aperture Trapping Potential

Supplementary figure S5 shows the calculated potential for the 56 nm aperture in manuscript Figure 1b. Manuscript figures 1a and 1b were patterned using the same design template, but they assumed different final dimensions due to dosage differences (3360 μC/cm2 for Fig. 1a and 3648 μC/cm2 for Fig. 1b) and fabrication variance. The 56 nm aperture exhibits the same dual minima characteristic as the calculated potential for the 38 nm aperture. Simulations show the minimum particle size this aperture can trap is 35 nm by

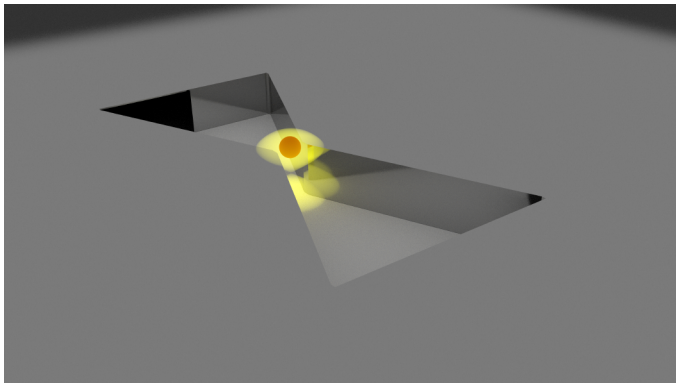

Figure S4: 3D schematic of our bowtie aperture.

overcoming k_BT of ambient thermal energy. However, as discussed in the main text, non-optical mechanisms such as van der Waals force and reduced particle degrees of freedom could enable trapping of smaller particles.

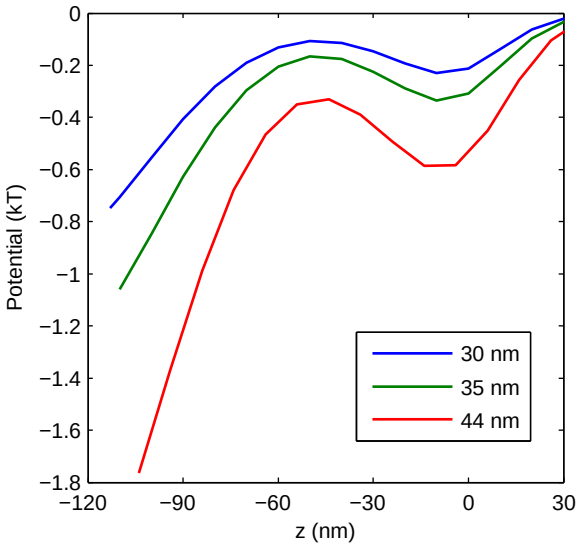

Figure S5: The calculated potential for particle trapping with the 56 nm aperture in manuscript figure 1b.

S4 Trap Stiffness Calculations

Supplementary figure S6 shows the optical force and intensity enhancement experienced by a 20 nm scQD along z and x axes in the 38 nm aperture from manuscript figure 1a. Note

that the force is positive at -25 nm (Sup. Fig. S6b), pulling the particle towards the front surface of the aperture. We calculated the z axis trap stiffness of 0.07 fN/nm/mW using the range from -60 nm to -80 nm where the change in force is steepest. The calculated x axis trap stiffness is 0.42 fN/nm/mW. The stiffness and force are larger along x axis because field is more confined in x-y plane.

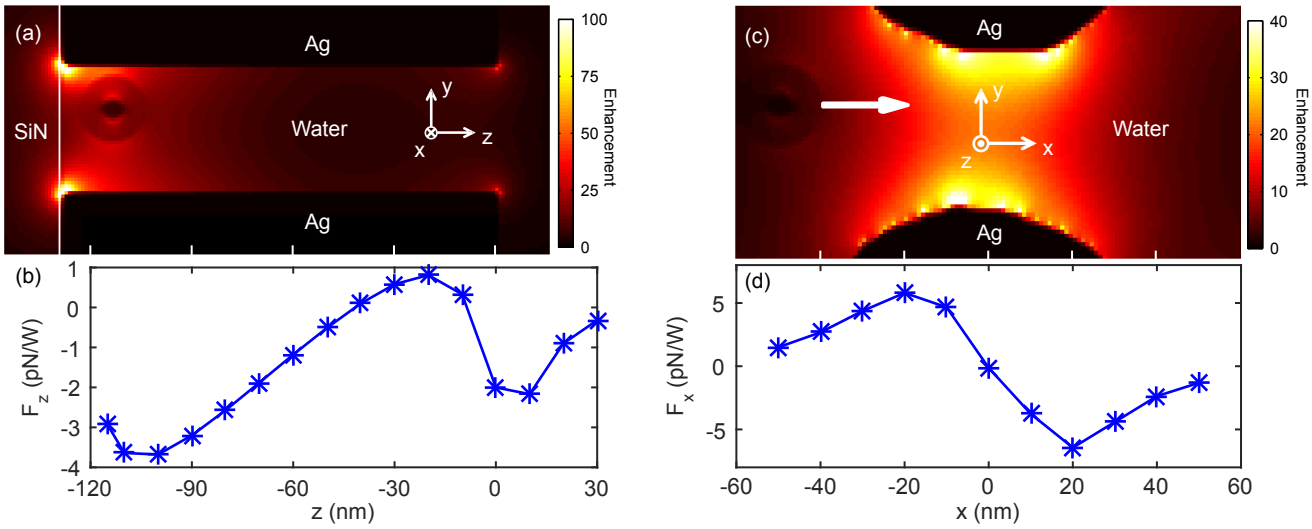

Figure S6: (a) The intensity enhancement and (b) force along the z axis. (c) The intensity enhancement and (d) force along the x axis. All forces are normalized to input power.

S5 Gradient Force Calculation and Comparison with Maxwell Stress Tensor

In order to understand whether our device operated in SIBA regime or not, we also performed the simulations using the gradient force formulation given by:

$$\langle \vec{F}_{\text{grad}}(r) \rangle \approx \pi \epsilon_e R^3 \frac{\epsilon_p - \epsilon_e}{\epsilon_p + 2\epsilon_e} \nabla |\vec{E}(r)|^2 \tag{S1}$$

where ϵ_p is the dielectric constant of the particle, ϵ_e the dielectric constant of the surrounding medium, and and R the radius of the particle. Comparing it with the results using Maxwell

Stress Tensor (MST) (Sup. Fig. S7), we can see with MST method the force is indeed larger, but the difference is really small, showing that our trapping is not close to SIBA regime yet. There is still space to improve our device trapping capability by making the particle take a more active role. The scattering force is 5 orders smaller than the gradient force, so we neglected it.

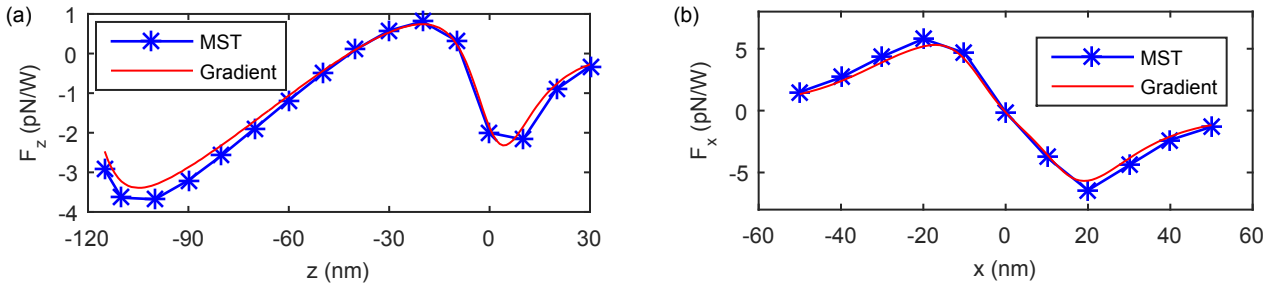

Figure S7: (a) (b) Comparison of the forces calculated by Maxwell Stress Tensor and Gradient force.

S6 Trapped Particle Emission Dynamics

Emission dynamics for two trapping experiments are shown in supplementary figure S8, with emission and transmission channels for the 56 nm gap aperture in S8a and S8b, and emission and transmission channels for the 38 nm gap aperture in supplementary figure S8c and S8d. Both experiments used filtered scQDs (Sup. Fig. S2) with a mean hydrodynamic diameter of 21.1 nm. Successful trapping of particles smaller than the minimum size predicted by force calculations in both of these apertures can be rationalized by two possible explanations. Firstly, non-optical mechanisms described in the main text may contribute to trapping. Secondly, the trapped particle size could lie in the tail end of the size distribution as determined by DLS measurements (Sup. Fig. S2), which extends out to 45 nm in diameter for the filtered particles.

The first trapping experiment using the 56 nm aperture shows an increase in 1064 nm trapping laser transmission at 200 seconds (Sup. Fig. S8b), indicating particle trapping.

The corresponding emission trace (Sup. Fig. S8a), however, does not exhibit emission until 260 seconds into the experiment, which is intermittent and resembles QD blinking. The second trapping experiment using the 38 nm aperture shows initial trapping in both the 1064 nm transmission (Sup. Fig S8d) and the emission (Sup. Fig S8c) at 210 seconds into the experiment. Subsequent trapping events, however, show subtle increases in 1064 nm transmission at 265 and 280 seconds, with corresponding emission events that rapidly decay in intensity after trapping. They all have similar increase both in fluorescence and transmission signal, most probably due to individual quantum dots trapped. We believe that it is unlikely that this situation could be due to three different aggregates.

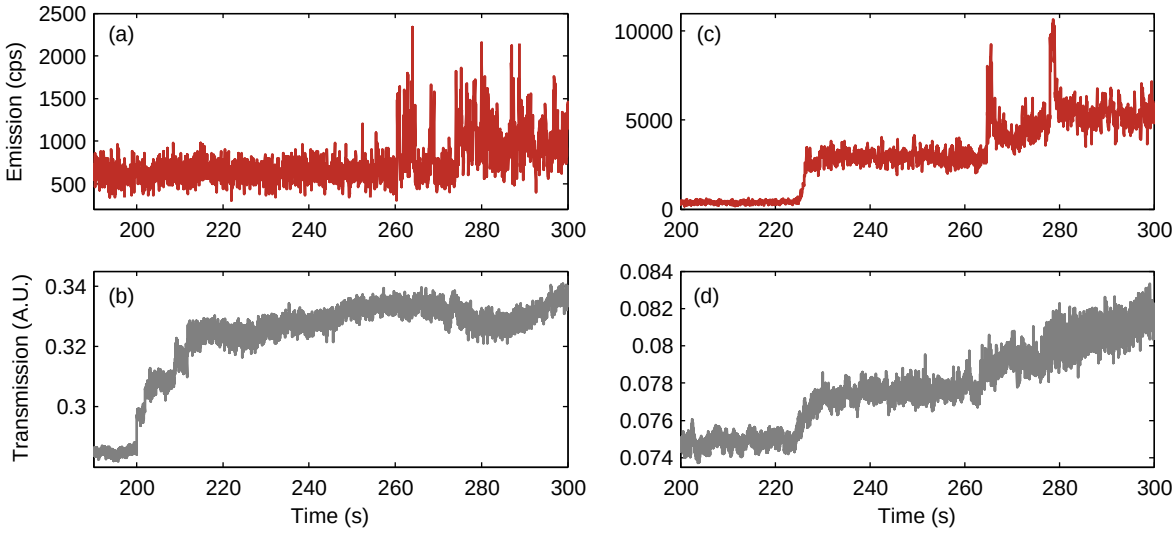

Figure S8: (a) Emission and (b) 1064 nm transmission for filtered scQDs in the 56 nm aperture shows evidence to QD blinking inside the optical trap. Multiple trapping events are detected in the (c) emission and (d) 1064 nm transmission channels for filtered scQDs in the 38 nm aperture that exhibit rapid quenching at 265 and 280 seconds in the emission channel only.

S7 Spectrally Detected Trapping Event

The emission and the transmission channels for the trapping event in manuscript figure 5 are shown in supplemental figure S9. The emission intensity was calculated by summing the

spectral intensity of each frame from spectrometer/CCD camera detection scheme. Spectra were collected with 1 second integration times, resulting in poor time resolution in the emission channel. Trapping occurred at 279 seconds and was stable until the trial ended at 300 seconds.

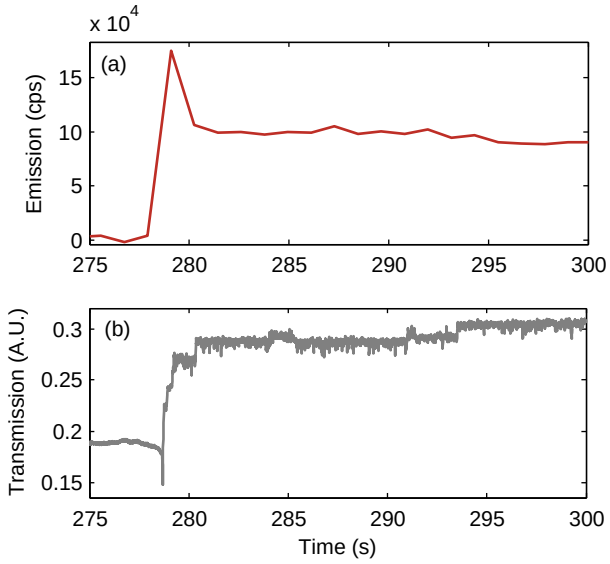

Figure S9: (a) Emission and (b) 1064 nm transmission channels for spectrally resolved emission detection presented in manuscript figure 5.

S8 Two-photon Photoluminescence of QDs on Silver Film

The most direct evidence to prove the QD inside the trap undergoes two-photon excitation is measuring the power dependence of the Two-photon Photoluminescence (TPPL). We measured the power dependence when QDs were drop-coated on the same silver film. Due to local electric field enhancement, the QD still emitted fluorescence under the illumination of the 1064 nm trapping laser. The squared dependence of the input power shows that the excitation was indeed due to two-photon excitation (Sup. Fig S10). Since the apertures feature much higher optical intensity than silver film, two-photon excitation becomes even

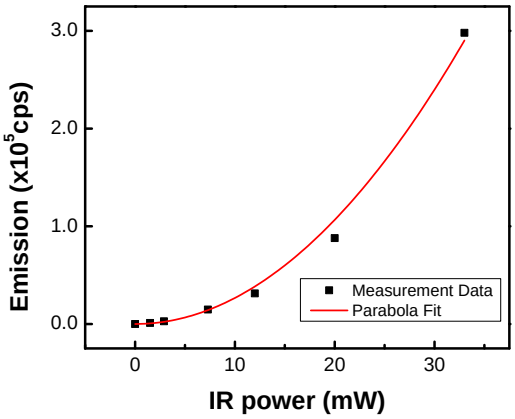

Figure S10: The fluorescence intensity versus input power, showing the squared dependence.

more likely. Therefore, based on this indirect measurement, we conclude that our luminescent data is indeed due to TPPL.

References

(1) Chen, O.; Zhao, J.; Chauhan, V. P.; Cui, J.; Wong, C.; Harris, D. K.; Wei, H.; Han, H.-S.; Fukumura, D.; Jain, R. K.; Bawendi, M. G. Compact high-quality CdSeCdS coreshell nanocrystals with narrow emission linewidths and suppressed blinking. *Nat Mater* **2013**, *12*, 445–451.

(2) Chen, O.; Chen, X.; Yang, Y.; Lynch, J.; Wu, H.; Zhuang, J.; Cao, Y. C. Synthesis of MetalSelenide Nanocrystals Using Selenium Dioxide as the Selenium Precursor. *Angewandte Chemie International Edition* **2008**, *47*, 8638–8641.